ACS OMEGA

Open Access

http://pubs.acs.org/journal/acsodf

Article

Study on the Self-assembly Behavior of Polycaprolactone Star-Shaped Copolymers Based on Dissipative Particle Dynamics

Jiashu Pan, Haiming Wang, Zijun Liu, Dengbang Jiang,* and Mingwei Yuan*

Cite This: *ACS Omega* 2025, 10, 15419−15431

Read Online

ACCESS | Metrics & More | Article Recommendations | Supporting Information

ABSTRACT: In this study, the pH-responsive self-assembly behavior of polycaprolactone star-shaped block copolymers in aqueous solution was systematically investigated by dissipative particle dynamics. The changes in morphology during the self-assembly process were studied by adjusting the number of polymer star arms, the degree of ionization of the terminal carboxylic acid group, and the concentration of the polymer in the solution. The results show that during the self-assembly process, the star-shaped copolymers undergo a series of structural transformations from spherical micelles to worm-like micelles and then to lamellar micelles as ionization and solution concentration change. When the degree of ionization is high, the electrostatic repulsion is enhanced, resulting in the formation of smaller spherical micelles; in contrast, when the degree of ionization is low, the electrostatic repulsion is weakened, resulting in the formation of larger and more complex worm-like or lamellar structures. With an increase in the number of arms, the self-assembly behavior of the system gradually transitions from complex morphologies (such as lamellar micelles and branched worm-like micelles) to simple morphologies (such as linear worm-like micelles and spherical micelles). This study provides important theoretical references and practical guidance for revealing the regulatory mechanisms of carboxyl ionization, the number of polymer star arms, and solution concentration on the self-assembly behavior of amphiphilic block copolymers.

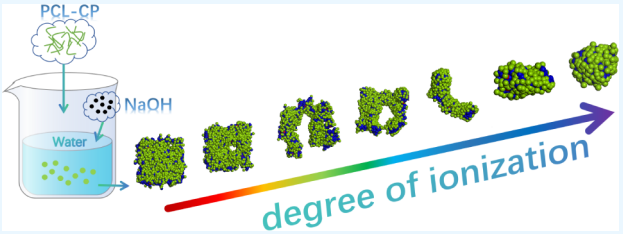

INTRODUCTION

With the development of drug delivery technology, nanodrug delivery systems have attracted much attention due to their ability to improve drug solubility, prolong blood circulation time, and enhance targeted delivery effects.[1−3] Star-shaped micelles based on biobased materials have become a highly regarded nanodrug delivery platform due to their structural diversity, environmental response, and excellent biocompatibility.[4−6] Through rational design, star-shaped micelles can achieve efficient drug loading and controlled release in specific microenvironments in vivo and in vitro, especially showing great potential in areas such as tumor treatment. For example, in the tumor microenvironment, cancer cells usually exhibit acidic characteristics. By designing polymers that are sensitive to acidic environments, precise drug release can be achieved.[7] In addition, the controllable synthesis and functional modification of such materials have further enhanced their research value and application prospects in the field of drug delivery.[8,9]

Compared with traditional linear block copolymers, biodegradable star-shaped block copolymers exhibit more complex and controllable self-assembly properties in solution due to their topological structures.[10−12] Star-shaped block copolymers not only have higher molecular weights and dense functionalization sites, but also provide unique self-assembly behaviors and higher molecular design freedom through the synergistic effect of multiarm segments. This structural advantage combined with biodegradable properties provides a way to prepare functional micelles with high performance and environmental friendliness.[13] Biodegradable star-shaped block copolymer micelles are usually composed of hydrophobic biodegradable segments (such as polycaprolactone (PCL), polylactic acid (PLA) or polyglycolic acid (PGA)) and hydrophilic segments (such as polyethylene glycol (PEG) or poly(ethylene oxide) (PEO)).[14−16] By precisely controlling the ratio of hydrophilic and hydrophobic segments, block length, and number of branches, star-shaped block copolymers can form a variety of nanostructures, such as spherical micelles, worm-like micelles, and vesicles. The core−shell structure formed by self-assembly exhibits excellent stability and loading capacity at the nanoscale. The hydrophobic core provides an efficient carrier space for hydrophobic drugs or functional molecules, while the hydrophilic shell can prolong the circulation time of micelles in the physiological environment, reduce nonspecific adsorption and immune recognition, and thus improve delivery efficiency.[17−20] In addition, due to the

Received: January 3, 2025
Revised: March 21, 2025
Accepted: March 25, 2025
Published: April 8, 2025

https://doi.org/10.1021/acsomega.5c00083
ACS Omega 2025, 10, 15419−15431

uniqueness of the star-shaped structure, this type of micelle usually exhibits a low critical micelle concentration (CMC), allowing it to maintain a stable micelle state even at low concentrations, thus being applied in actual biological environments.[21] In practical applications, the degradation products of these biobased polymers are often nontoxic and can be eliminated through human metabolic pathways. This feature effectively avoids the bioaccumulation or toxicity problems that may be caused by traditional polymer materials, thereby significantly enhancing their application potential in biomedicine and environmental sciences. Taking polycaprolactone as an example, its degradation product 6-hydroxycaproic acid can be further metabolized into carbon dioxide and water, ensuring the safety and eco-friendliness of the material.[22]

However, although biodegradable star-shaped block copolymer micelles have shown great application potential, the relationship between their structural design and performance regulation remains a key issue in research.[23−25] For example, the specific influence mechanism of block ratio, segment length, arm number and topological structure on micelle stability and self-assembly behavior is not fully understood, and the dynamic self-assembly process cannot be clearly observed using microscopy and scattering techniques. In this context, the rapid development of computational simulation techniques, especially self-consistent field theory (SCFT) and dissipative particle dynamics (DPD), has played an irreplaceable role in exploring the self-assembly mechanism of star-shaped block copolymers.[26] SCFT is a classical theoretical tool for studying the phase behavior of block copolymers, and is capable of accurately predicting the evolution of the polymer phase diagrams and micromorphology. Its deterministic solution avoids the statistical rise and fall problem and can resolve the effects of different block compositions, chain lengths, and interaction parameters on the phase behavior.[27] SCFT combines analytical and numerical calculations to systematically construct the phase diagrams and reveal the microphase segregation and ordered-disordered phase transitions. The method is widely used in polymer science, successfully predicting experimentally observed morphologies and providing a solid foundation for the theoretical design of block copolymers.[28] DPD, as a mesoscopic-scale coarse-grained simulation method, is centered on describing interparticle interactions by simultaneously introducing conservative, dissipative and random forces. It has significant advantages in studying the self-assembly of block copolymers and their aqueous solution morphology, including the ability to simulate large and long time scale systems, capture polymer dynamics behavior, describe structural evolution in complex environments, and reproduce experimentally observed morphologies while maintaining sufficient computational efficiency. In contrast, SCFT is mainly suitable for accurate prediction of equilibrium microphase-separated structures, but has limitations in describing nonequilibrium dynamical processes. However, the DPD method still faces some challenges, such as the calibration of the interaction parameters relies on a reasonable mapping of the Flory−Huggins parameters, the coarse-grained model may lose some of the molecular details, and the accuracy in the simulation of complex morphologies of macromolecules is limited by simplifications of the interparticle interactions. Current research focuses on optimizing the DPD force field parameters, improving the model's fit to experimental data, combining with other computational methods (SCFT or all-atom/coarse-grained MD) to obtain more accurate self-assembly predictions, and exploring its applications in areas such as drug delivery and soft-matter material design, in order to further enhance its reliability and applicability in the simulation of polymer systems. Through DPD simulation, researchers can clearly reveal the formation process of block copolymers in different solvent environments, the formation process of core−shell structures, and the microphase separation mechanism between different segments. In addition, DPD can also quantify the influence of key parameters (such as segment hydrophilicity, block ratio and number of branches) on the final self-assembly morphology, laying the foundation for experimental design.[29,30] Researchers have conducted extensive research on the dynamic process of polymer self-assembly through DPD simulation. Yang[31] and his team experimentally studied the application of disulfide-linked polycaprolactone-*b*-polyethylene glycol methyl ether methacrylate in doxorubicin (DOX) delivery. Based on DPD simulation technology, they effectively verified that the developed DPD simulation method can describe the reduction reaction of dynamic covalent bond cleavage and the self-assembly behavior of drug-loaded polymer micelles. Xu et al.[32] used dissipative particle dynamics simulation technology to explore the effect of solution pH on self-assembly structure and the role of hydrophilicity of pH-responsive microspheres in the transformation of single-molecule micelles. Zheng et al.[33] studied the aggregation behavior of pH-sensitive amphiphilic polymer micelles poly(methyl methacrylate-*co*-acrylic acid)-*b*-poly(polyethylene glycol methyl ether monomethacrylate) self-assembly through DPD simulation. The simulation results were consistent with the experimental results. This research strategy combining theory and experiment can not only deepen the understanding of the complex self-assembly mechanism of star-shaped block copolymers but also provide a scientific basis for the development of new functional materials.

In response to Pranav's[34] study on biodegradable star-shaped block polycaprolactone micelles, star-shaped block copolymers with different structures were synthesized by two-step ROP by keeping the arm length constant and changing the number of arms to explore their self-assembly behavior and potential application in drug delivery. This study focuses on the self-assembly behavior of pH-responsive star-shaped brush-shaped polycaprolactone block copolymers in this experiment. Through dissipative particle dynamics (DPD) and molecular dynamics (MD) simulation methods, the self-assembly behavior of pH-responsive biobased polycaprolactone star-shaped brush-shaped block copolymers is systematically explored by the effects of ionization degree, concentration and arm number. The microphase separation behavior of PCL-CP molecular aggregates forming spheres, cones or truncated cones in aqueous solution is fully revealed. It provides theoretical support for understanding the self-assembly behavior of star-shaped brush-shaped block copolymers and stimulates the application potential of pH-responsive materials in the field of drug delivery.

DPD SIMULATION

DPD Simulation Method. In 1992, Koelman and Hoogerbrugge[35] first established a new computational method that is more suitable for fluid dynamics behavior. DPD simulation is a mesoscopic simulation method suitable for studying the self-assembly behavior, drug distribution and drug

https://doi.org/10.1021/acsomega.5c00083
ACS Omega 2025, 10, 15419−15431

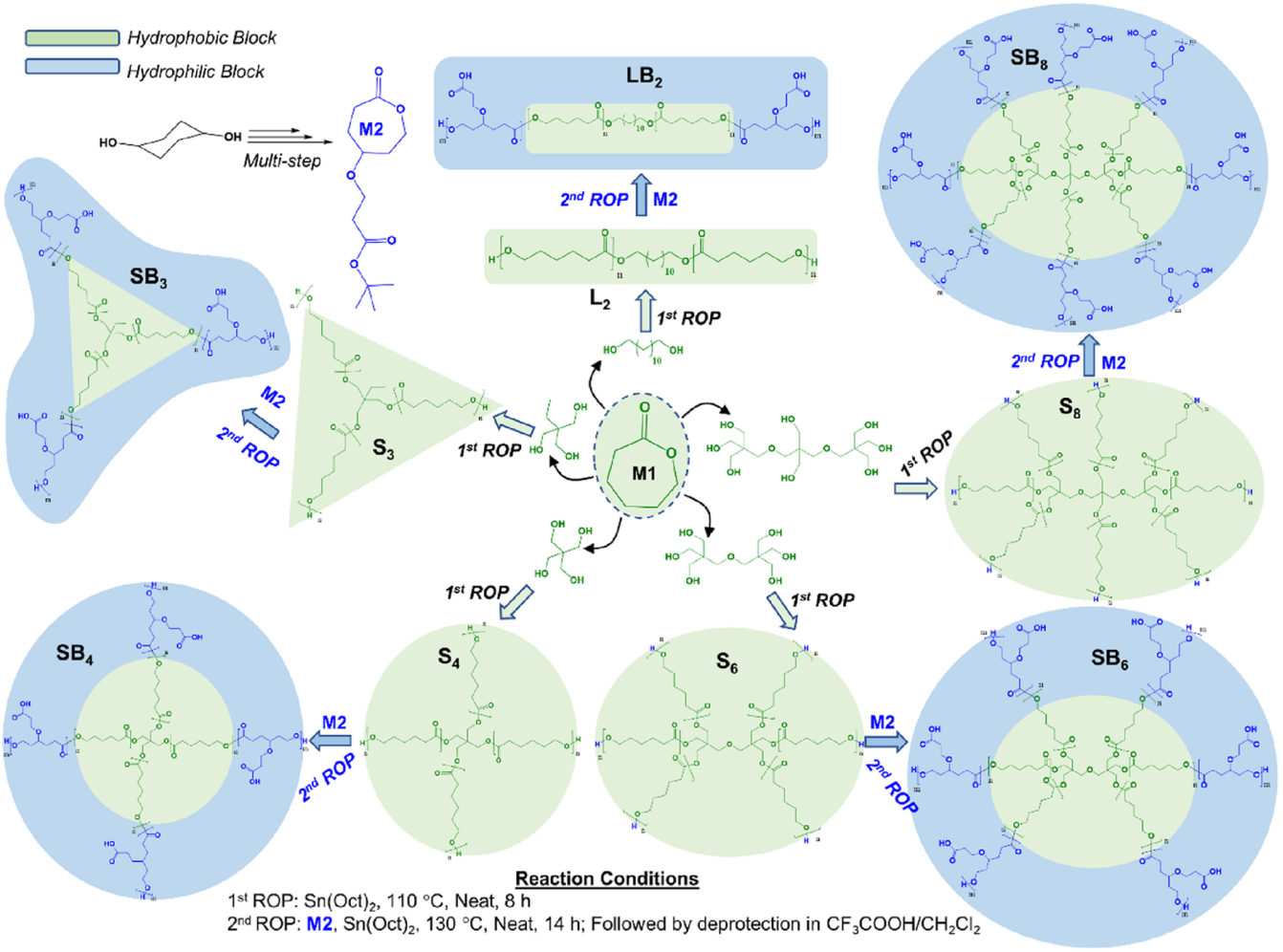

Figure 1. Synthesis route of PCL-*b*-M2 star-shaped block copolymer (PCL-CP) by Pranav et al.[34] Reprinted with permission from Pranav et al.[34] Copyright {2023} American Chemical Society.

release process of drug-loaded polymer micelles. Its calculation principle is to divide the entire polymer molecular chain into several fragments of similar volume size, which are generally called coarse-grained beads. These microspheres are usually large at the nanoscale and small at the macroscale, and are a mesoscopic simulation method.[36,37] Therefore, in DPD simulation, in order to avoid a lot of computational work, the degrees of freedom between particles are not considered, and only the movement of the center of mass is considered, but the important microstructural characteristics and dynamic motion behavior trajectory are conserved.

$$\frac{d\vec{r}_i}{dt} = \vec{v}_i \tag{1}$$

$$m_i = \frac{d\vec{r}_i}{dt} = \vec{F}_i \tag{2}$$

In the above formula, m_i, $\vec{r}_i$,$\vec{v}_i$ represents the mass, coordinates and velocity of the microbeads. The force ($\vec{F}_{ij}$) between each pair of microbeads is the sum of conservative force ($\vec{F}_{ij}^{C}$), dissipative force ($\vec{F}_{ij}^{D}$), random force ($\vec{F}_{ij}^{R}$), elastic force ($\vec{F}_{ij}^{S}$) and electrostatic force ($\vec{F}_{ij}^{E}$), given by the following formula:

$$\sum_{i\neq j}^{n} (\vec{F}_{ij}^{C} + \vec{F}_{ij}^{D} + \vec{F}_{ij}^{R} + \vec{F}_{ij}^{E} + \vec{F}_{ij}^{S}) = \vec{F}_{ij} \tag{3}$$

Among them, the conservation force $\vec{F}_{ij}^{C}$ is a flexible repulsive force along the center line, which is linearly related to the distance between the microbeads and decreases linearly with the increase of the distance between the microbeads; the dissipation force $\vec{F}_{ij}^{D}$ represents the mutual friction between the microbeads, that is, the energy consumption of the system, which is proportional to the relative speed between microbeads i and j; the random force $\vec{F}_{ij}^{R}$ provides energy for the system, which just compensates for the reduction of degrees of freedom caused by the coarse-graining of the system. All forces disappear after a certain cutoff radius Rc, which is usually set to 1 unit length in the simulation.[38,39] The three forces can be obtained by the following formulas:

$$\vec{F}_{ij}^{C} = \begin{cases} \alpha_{ij}(1 - r_{ij})\vec{r}_{ij}r_{ij}, & r_{ij} < 1 \\ 0, & r_{ij} \geq 1 \end{cases} \tag{4}$$

$$\vec{F}_{ij}^{D} = -\frac{\sigma^2(\omega(r_{ij}))^2}{2kT}(\vec{r}_{ij}\cdot\vec{v}_{ij})\vec{r}_{ij} \tag{5}$$

https://doi.org/10.1021/acsomega.5c00083
ACS Omega 2025, 10, 15419−15431

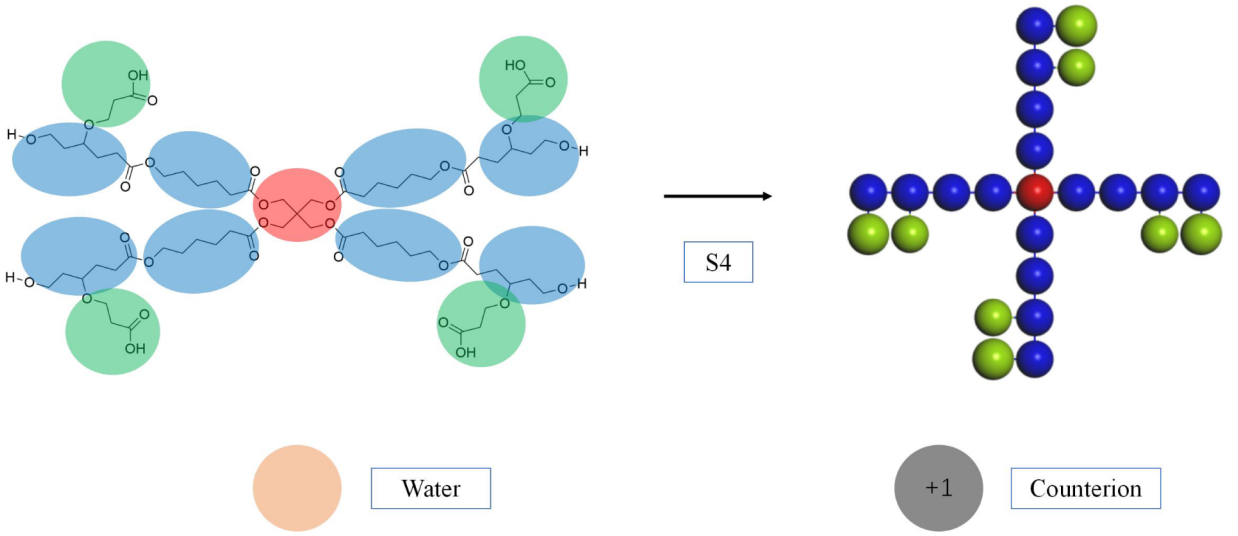

Figure 2. S4 granularization model diagram.

$$\vec{F}_{ij}^{R} = -\frac{\sigma\omega(r_{ij})\vec{r}_{ij}\xi_{ij}}{\sqrt{\delta_t}} \quad (6)$$

In the above formula, α_{ij} is the interaction parameter between microbeads i and j, $\vec{r}_{ij} = \vec{r}_i - \vec{r}_i$, $r_{ij} = |\vec{r}_{ij}|$, $\vec{v}_{ij} = \vec{v}_i - \vec{v}_j$, ξ_{ij} is a random fluctuation variable with a mean value of 0 and a unit variance of 0, σ is the random force intensity, k is the Boltzmann constant, T is the system temperature, δ_t is the simulation time step, ω is the weight function related to r and disappears when r > 1.

The model of electrostatic interaction adopts the smearing charge method with an exponentially decaying Slater-type charge density distribution. Where λ_e is the decay length of the charge

$$f(r) = \frac{q}{\pi\lambda_e^3}\exp\left(-\frac{2r}{\pi\lambda_e^3}\right) \quad (7)$$

The electrostatic force and electrostatic energy between microbeads i and j are expressed by the following formula:

$$\vec{F}_{ij}^{E} = \frac{q_i q_j}{4\pi {r_{ij}}^2}\lambda_B\left[1 - \exp\left(\frac{-2r_{ij}Rc}{\lambda_e}\right)\left(1 + \frac{2r_{ij}Rc}{\lambda_e\left(1 + \frac{r_{ij}Rc}{\lambda_e}\right)}\right)\right]\frac{\vec{r}_{ij}}{r_{ij}} \quad (8)$$

$$U_{ij}^{E} = \frac{q_i q_j}{r_{ij}}\lambda_B kT[1 - (1 + \beta r_{ij})e^{-2\beta r_{ij}}] \quad (9)$$

In the above equation, Groot[40] obtained $\beta = 1.356$ by substituting the electrostatic interaction between the two charge density distributions at $r_{ij} = 0$, and then obtained $\lambda_e = 0.737$ from the relationship $\beta = Rc/\lambda_e$. In addition, we also determined $\lambda_B = 0.75$, the cutoff value $r_c = 3$, and the real space convergence parameter $\alpha^{ES} = 0.975$ when using PPPM and treating long-range electrostatic interactions.

The hydrophilicity of polymer microbeads is determined by the repulsive force parameter (a_{ij}). Therefore, it is crucial to determine the repulsive force parameter between different types of microbeads. The a_{ij} between DPD microbeads i and j depends on the potential atomic interactions that are linearly related to the Flory–Huggins parameter (χ_{ij}), as follows.

$$\alpha_{ij} = \alpha_{ii} + 3.5\chi_{ij} \quad (10)$$

Here, when density $\rho = 3$ and $k_BT = 1$, $\alpha_{ii} = 25k_BT$ (Groot and Warren showed that $\rho = 3$ and $\alpha_{ii} = 25k_BT$ are basic parameters of the solution), and a can be calculated based on the solubility parameter using the following formula.

$$\chi_{ij} = \frac{(\delta_i - \delta_j)^2 v}{RT} \quad (11)$$

where V is the arithmetic mean of the molar volumes of beads i and j, and δ_i and δ_j are solubility parameters that depend on the chemical properties of the beads and can be obtained by molecular dynamics (MD) simulations.

DPD Model Establishment and Parameter Debugging. As shown in Figure 1, the construction of polymer micelles (PCL-CP) in the experimental study of Pranav[34] is based on small molecule polyols (1,12-dodecanediol, 2-bis(hydroxymethyl)-butanol, pentaerythritol, dipentaerythritol, tripentaerythritol) as initiators, ring-opening polymerization (ROP) of caprolactone monomers as hydrophobic layers, and then the polymer polyols are used as initiators, and γ-carboxycaprolactone monomers are ring-opening polymerization as hydrophilic layers. Figure 2 Coarse-grained modeling diagram showing the mapping of S4 polymer micelle chains and DPD microbeads. During the self-assembly process, the copolymer is divided into three types of microbeads: PCL (blue), B (red) and CP (green). 33 water molecules are represented as a water microbead W (orange). The counterion is a free ion with a valence of +1 (black). The categories of B (red) include two-arm (S2 microbeads), three-arm (S3 microbeads), four-arm (S4 microbeads), six-arm (two S4 microbeads), and eight-arm (three S4 microbeads). This paper studies the coarse-grained models of 5 arm numbers.

In this study, the molecular dynamics module of Lammps software was used to calculate the interaction parameters using COMPASS III force field. The main simulation parameters are as follows: the energy convergence threshold is 1.0×10^{-4} kcal·mol^{-1}, and the force convergence threshold is 0.005 kcal·mol^{-1}·Å^{-1}. The calculation cutoff radius value of van der Waals

https://doi.org/10.1021/acsomega.5c00083
ACS Omega 2025, 10, 15419−15431

Table 1. Interaction Parameter a_{ij} Used in the DPD Simulation

	PCL	CP	B4	W	B2	B3	Counterion
PCL	25						
CP	64.90	25					
B4	25.71	29.31	25				
W	70.60	26.05	39.70	25			
B2	18.13	70.75	-	45.57	25		
B3	30.60	67.56	-	26.30	-	25	
Counterion	70.60	26.05	39.70	25	45.57	26.30	25

force is 15.5 Å, the spline width is 0 Å, and the buffer width is 2 Å. The interaction parameters a_{ij} calculated by MD simulation are shown in Table 1:

In this study, the pH value of the solution was qualitatively designed by changing the degree of ionization (α) of the carboxyl-terminated microbeads according to the treatment method proposed by Procházka.[41] The dissociation constant (K_A) of the electrolyte solution and the relationship between α were approximately calculated (eqs 12 and 13). In actual molecular simulations, accurate treatment of charge balance is very important. In theory, to ensure the overall electrical neutrality of the system, the charge balance is 0. Therefore, by adding additional counterions qc = ±1, and then using charge correction technology (in some high-precision simulations, the charge correction algorithm can be used to adjust the charge distribution of the system to ensure a more accurate charge balance). The role of counterions is to form an ionic atmosphere on the surface of the micelles, which plays an electrostatic shielding role. This shielding effect can not only reduce the electrostatic repulsion between the end group ions of the surfactant and affect the charge balance of the micelles, but also affect the overall self-assembly behavior of the system.[42] Different types and concentrations of counterions will change the critical micelle concentration (CMC) of the micelles, the type of micelles formed (such as spherical, cylindrical or lamellar structures), and the stability of the micelles. Therefore, the ionization degrees in this study are α = 0, 0.05, 0.1, 0.2, 0.4, 0.8, and 1.0, respectively.

$$pH - pK_A = lg\frac{\alpha}{1-\alpha} + lg\gamma_{DH} \quad (12)$$

$$lg\gamma_{DH} = -0.509\sqrt{I} \quad (13)$$

In the above formula, the influence of the activity coefficient of monovalent ions in the Debye−Huckel limiting formula theory is taken into account. The approximate mapping relationship between α and pH value is shown in Table 2.

Table 2. Approximate Mapping of α to pH

α	0.05	0.1	0.2	0.4	0.8
pH-pK_A	−1.279	−0.954	−0.602	−0.176	0.602

DPD simulations were performed using GROMACS. The main simulation parameters are as follows: The volume of a bead is approximately 988 Å^3. To ensure that the physical density corresponds to the simplified density ρ = 3 from which the correlations were derived, the length scale must be reset. Therefore, the three beads occupy a volume of 3 × 988 = 2964 Å^3, corresponding to a cube with an edge of $2964^{(1/3)}$ = 14.36 Å (Rc). This value must be chosen as the cutoff radius between two beads to match the desired physical density and the simplified density. Half of the length scale, which is the radius of each bead (7.18 Å), can be used to display the bead radius. In the DPD simulation, we chose a cubic box of 20 × 20 × 20 R3 C (280 × 280 × 280 Å^3). In order to achieve thermodynamic equilibrium, each simulation was performed with a time step of 1.0−1.5 × 10^5 (118245.01−177367.51 ps), a step size of Δt = 0.05 (1182.45 fs), a calculated cutoff radius value of the van der Waals force of 14.36 Å, a mass scale of 672 amu, an energy scale of 0.59219 kcal·mol^{-1}, a spline width of 0 Å, a buffer width of 2 Å, a dissipation strength of 4.5 (0.12787 amu/fs), and a spring constant of 4.0.

RESULTS AND DISCUSSION

Phase Diagram of Multiarm Micelle Self-assembly. In order to more comprehensively understand the self-assembly motion trajectory of multiarm star-shaped micelles, we drew the two-dimensional phase diagram of the concentration (C)-ionization degree (α) of S2, S3, S4, S6, and S8. It can be seen from Figure 3 that the morphology changes within the range of the abscissa α (0, 0.05, 0.1, 0.2, 0.4, 0.8, 1) and the ordinate C (0.05, 0.08, 0.11, 0.14, 0.17, 0.20). The legend marks four different self-assembly morphologies: lamellar micelles (green squares), branched worm-like micelles (blue triangles), linear worm-like micelles (yellow inverted triangles) and spherical micelles (red dots). Analysis of the information in the figure: PCL-CP micelles are weakly hydrophilic and strong hydrophobic at low ionization degrees. The interaction between hydrophobic segments in the system dominates, and they are more inclined to form high-dimensional complex Morphology (e.g., lamellar and branched worm-like micelles). As the degree of ionization increases, the hydrophilicity increases significantly and the aggregation between hydrophobic segments weakens. At this time, the system tends to form a more symmetrical and simple structure (such as spherical micelles). The influence of changes in the number of arms on each morphology is analyzed below from three aspects: geometric constraints, steric repulsion effects and free energy minimization.

The Influence of Geometric Constraints. The low arm number system (S2, S3) has low geometric symmetry and less restricted stacking between chain segments, which gives the molecules a higher degree of deformation freedom, making it easier to form complex lamellar or branched worm-like micelles. These morphologies are mainly distributed in low ionization and high concentration regions, and the molecular morphology is closer to linear blocks, with weaker geometric constraints during stacking. With the increase in the number of arms, the molecular symmetry and volume occupancy of the high arm number system (S6, S8) increase, which strengthens the geometric constraints, thereby limiting the formation of complex morphologies (such as lamellar and branched micelles), and gradually transitioning to simple morphologies such as spherical and linear worm-like micelles. The S4 system

https://doi.org/10.1021/acsomega.5c00083
ACS Omega 2025, 10, 15419−15431

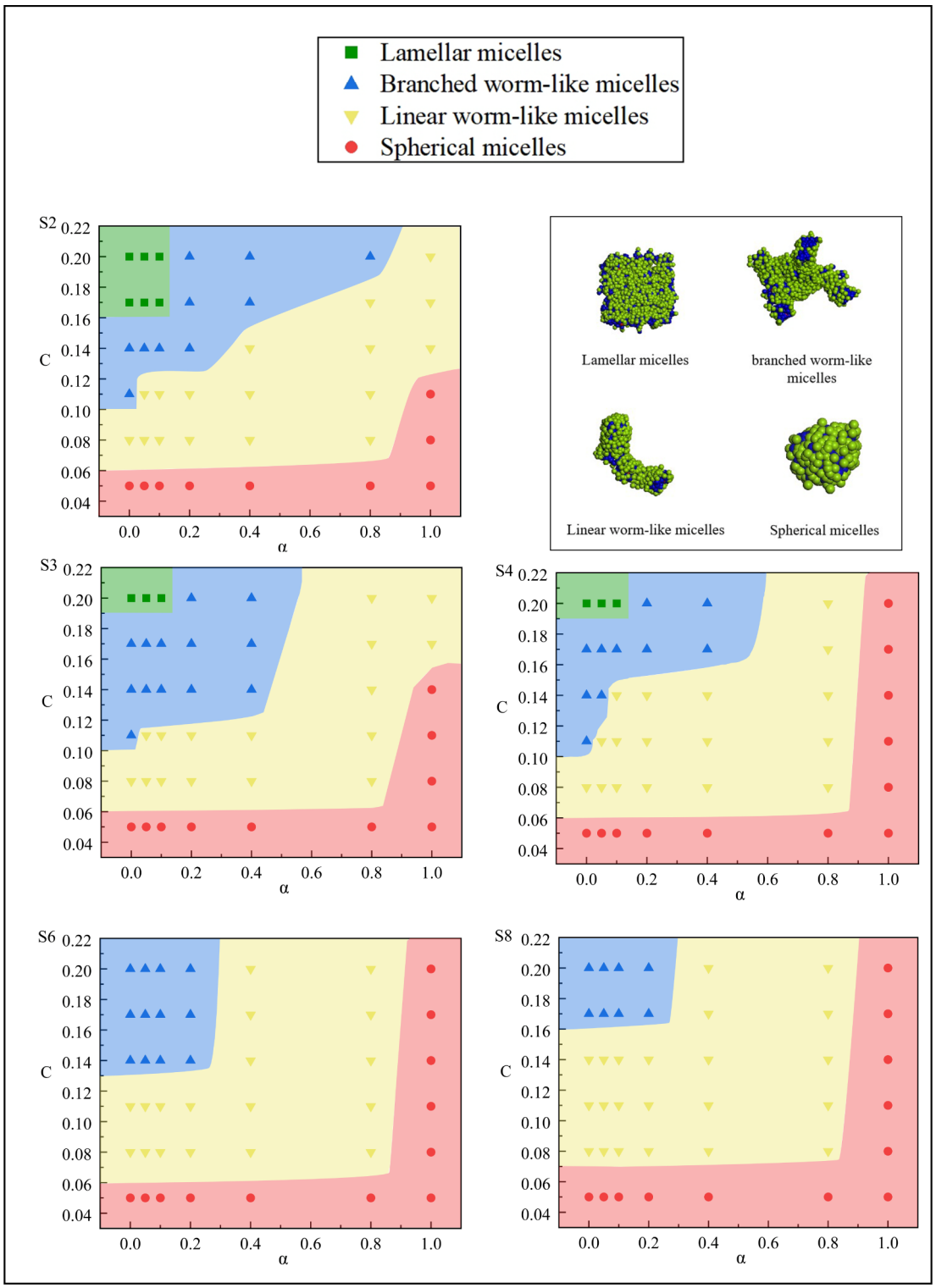

Figure 3. Concentration−ionization (C-α) phase diagrams of multiarm PCL-CP star-shaped block copolymers (S2: two-arm; S3: three-arm; S4: four-arm; S6: six-arm; S8: eight-arm).

in the transition state shows a balance between geometric morphology and degrees of freedom. Its morphological distribution contains certain complex structures and gradually tends to simple morphologies.

The Effect of Spatial Electrostatic Repulsion. Due to the weak steric repulsion of low-arm-number systems, the hydrophobic segments are more likely to accumulate in the concentrated area, forming complex structures such as sheet-like and branched micelles. In high-arm-number systems, the steric repulsion effect is significantly enhanced, especially in the concentrated region, where the intermolecular repulsion inhibits the stability of high-dimensional morphology. In contrast, spherical micelles can effectively reduce the steric repulsion effect due to their compact packing method, and show higher stability in systems with high arm numbers. The steric repulsion effect of the S4 system is between low and high

https://doi.org/10.1021/acsomega.5c00083
ACS Omega 2025, 10, 15419−15431

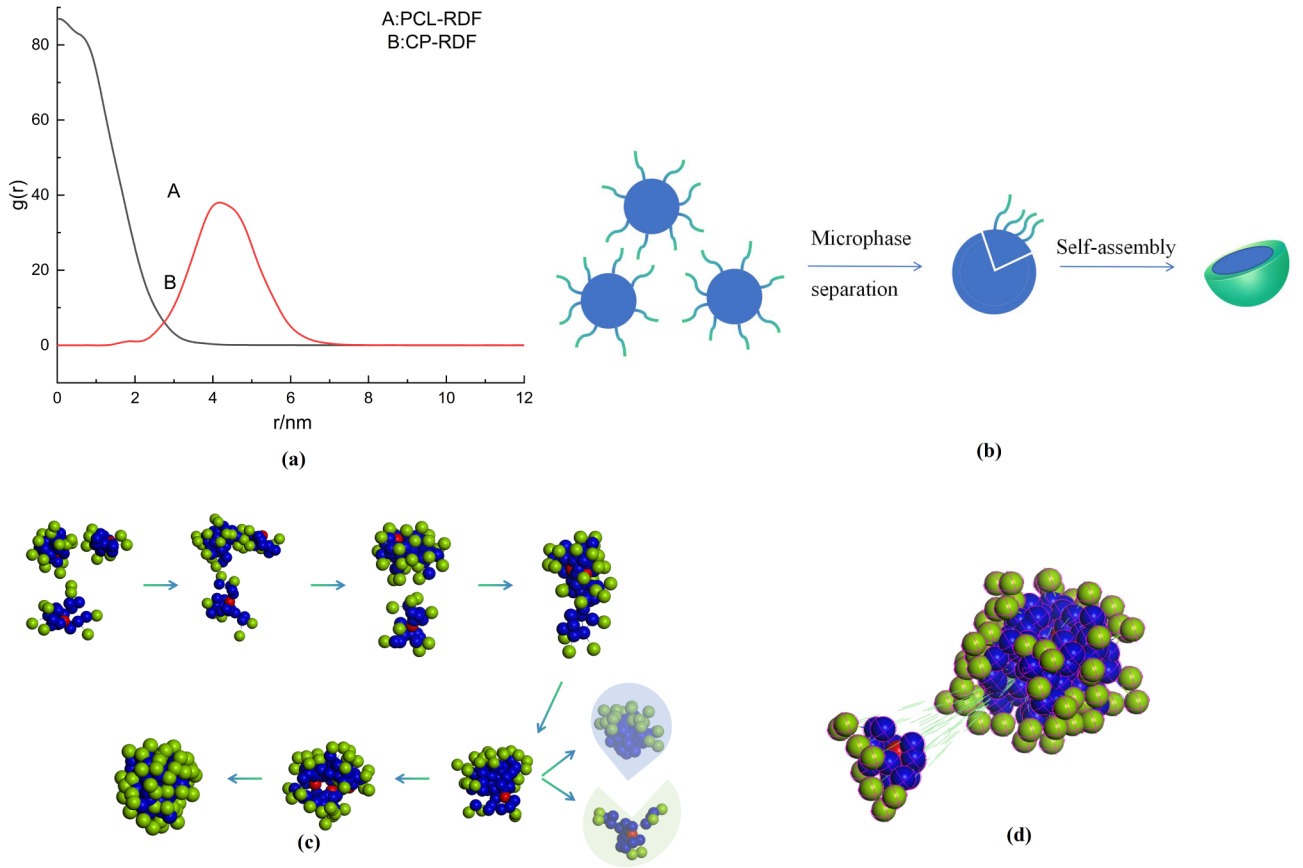

Figure 4. (a) Radial distribution function (RDF) of the distance from the center of mass for S4-(α = 1.0, C = 0.20) PCL(A), CP(B); (b) schematic formation of spherical micelles and molecular stacking models; (c) S4-(α = 1.0, C = 0.20) simulated snapshots of the self-assembly mechanism of the spherical micelles as well as localized decomposition maps; (d) schematic depth-cutting of PCL-CP spherical micelles.

arm numbers, giving it the ability to avoid too close packing while maintaining a certain complex morphology.

The Influence of Free Energy Minimization Drive. Low arm number systems have higher deformation freedom. Through the stacking effect of hydrophobic segments and the solvation of balanced hydrophilic segments, lamellar or branched micelles can be formed, thereby reducing the free energy of the system. In high arm number systems, simple forms (such as spherical or linear worm-like micelles) have lower free energy. The compact stacking of hydrophobic blocks and the minimization of the surface energy of hydrophilic blocks make spherical micelles the optimal structure for high arm number systems. The free energy drive of the S4 system takes into account the needs of segment stacking and the spatial repulsion effect, so that the linear worm-like micelles formed have the lowest free energy.

Overall Phase Diagram Trend Analysis. 1. With the increase of the number of arms, the self-assembly behavior of the system gradually transitions from complex forms (lamellar micelles and branched worm-like micelles) to simple forms (linear worm-like micelles and spherical micelles). This trend reflects that the increase in the number of arms will enhance the spatial repulsion between molecules and reduce the possibility of the system forming a complex structure. 2. The geometric symmetry and uniformity of the chain segment distribution of the high arm number system are improved, making it easier for the system to form low-dimensional, simple-morphology structures (such as spherical micelles). At the same time, the high arm number also provides higher flexibility and freedom for the chain segments, which helps to reduce the internal stress of the system and stabilize the simple morphology. 3. The change in the number of arms significantly affects the self-assembly behavior by regulating the geometric parameters of the polymer (such as the stacking mode of the hydrophobic block) and the energy of intermolecular interaction. This provides theoretical support for designing polymer materials with specific morphologies by adjusting the number of arms. By reasonably selecting the number of arms, precise regulation from lamellar micelles to linear worm-like micelles and then to spherical micelles can be achieved, laying the foundation for the development of functional materials. In order to reveal the self-assembly process of different types of aggregates and the molecular packing structure of the aggregates, they will be discussed in the following chapters.

Spherical Micelles. When not affected by the degree of ionization and the number of arms, dilute solutions (concentration below 8%) mainly exist as spherical micelles. We believe that this phenomenon is a balance between the electrostatic interaction of the terminal carboxyl groups and the van der Waals interaction of the hydrophilic and hydrophobic blocks in dilute solutions, that is, the concentration is the main influencing factor, and the distance between the micelle molecules can make the electrostatic interaction temporarily negligible. When the carboxyl groups are completely ionized into carboxyl ions (α = 1), the electrostatic repulsion of the terminal carboxyl groups increases with the increase of concentration. Under the dual influence of

https://doi.org/10.1021/acsomega.5c00083
ACS Omega 2025, 10, 15419−15431

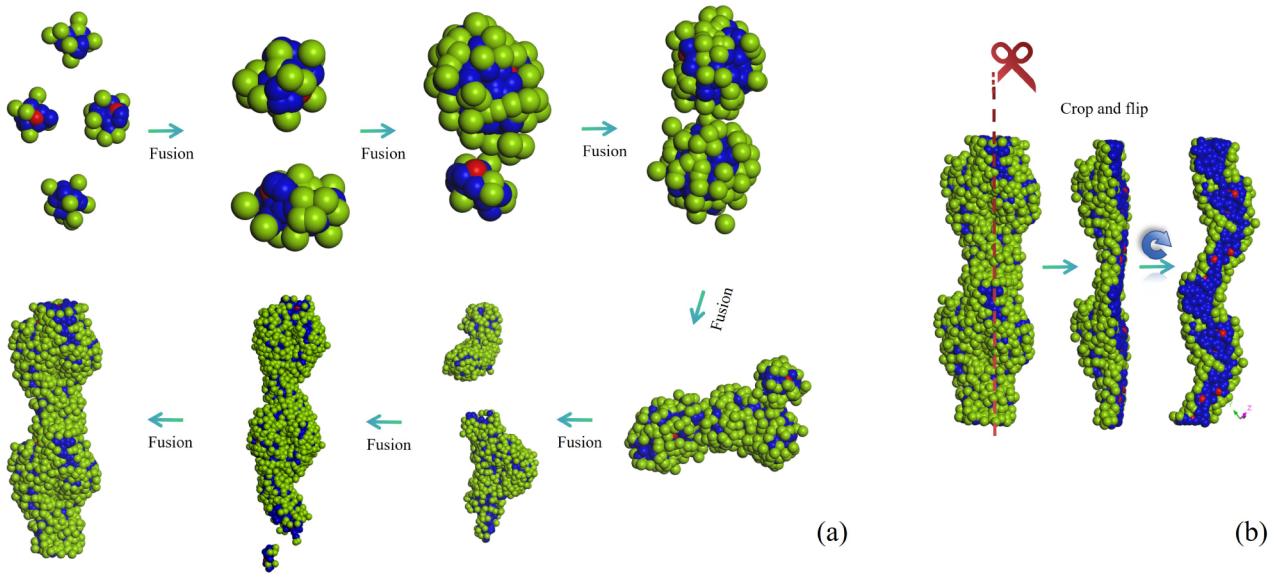

Figure 5. S4 (α = 0.1, C = 0.11). (a) The formation process of linear worm micelles. (b) Cross-section rotation diagram of linear worm-like micelles.

electrostatic interaction and van der Waals interaction, multiple PCL-CP molecules aggregate into spherical micelles.

Low arm number (S2, S3) system: Spherical micelles are formed in the low ionization region, but the distribution range is small and the stability is low. The flexibility between molecules is greater, and it is easier to form other complex forms (such as branched worm-like micelles or lamellar micelles); Transition arm number (S4) system: The distribution range of spherical micelles gradually expands, becoming one of the dominant forms in the system. As the number of arms increases, the molecular geometry tends to be symmetrical, and the spherical structure becomes the stable form with the lowest free energy; in high arm number (S6, S8) systems: spherical micelles have the widest distribution range in the entire phase diagram, the strongest stability, and become the dominant form. Under high ionization conditions, the formation of spherical micelles is easier and more stable, and the size is larger.

As the number of arms increases, the distribution range of spherical micelles continues to expand and eventually dominate the entire system. The reason is that the molecular geometric symmetry is enhanced, the free energy is minimized, and the repulsion is strengthened, which makes spherical micelles the most stable and optimal self-assembly form in high arm number systems.

PCL-CP molecules are uniformly dispersed in the solution and then quickly self-assemble into small aggregates. Subsequently, small spherical micelles fuse with neighboring small micelles or monomers to gradually form large spherical micelles, and finally the micelle size distribution reaches a dynamic equilibrium state. In addition, Figure 4a shows the radial distribution function of micelles with α = 1.0 and C = 0.20. We found that the micelle is composed of a core formed by aggregated hydrophobic PCL segments and an outer corona formed by hydrophilic CP segments. At a distance of 11 Å from the center of mass, the probability distribution of hydrophobic beads is greater than 89.8%, indicating that the hydrophobic beads are densely packed in the core, there are no hydrophilic beads and solvent in the core, and the remaining is the initiator core of the copolymer. In short, the PCL-CP polymer is completely microphase separated in the final micelle. Therefore, we call it a microphase-separated small spherical micelle. In Figure 4d, a PCL-CP spherical micelle is marked with different colors and is gradually microphase separated into a truncated cone geometry with separated cores and arms. Therefore, the self-assembly mechanism of spherical micelles can be summarized as Figure 4b,c. The corresponding dynamic process of spherical micelle self-assembly can be seen in the Video in the Supporting information.

Worm-like Micelles. Linear worm-like micelles present a long and thin linear morphology. When the molecules of this morphology of micelles are stacked, the chain segments are relatively long and remain linearly arranged, forming a worm-like structure. The self-assembly process of worm-like micelles was studied in S2, S3, S4, S6 and S8 molecules with α = 0 −1 and C = 0.08−0.20. Most of the micelles that can self-assemble into worm-like structures are generally divided into three structures: short rod-like worms, linear long worms and branched worms. As shown in Figure 5, linear worm-like micelles are usually formed by the aggregation of multiple block copolymer molecules through hydrophobic interaction, presenting a long linear structure similar to worms or rods. Its surface is usually covered by hydrophilic segments, while the hydrophobic segments are located in the core of the micelles to ensure the stability of the overall morphology. Compared with spherical micelles, linear worm-like micelles have greater flexibility and longer axial length, and usually form a looser structure. The whole process can be divided into four stages. Initially, randomly distributed PCL-CP molecules aggregate into microphase-separated spherical micelles. Then, these spherical micelles fuse with each other into short rod-like worm-like micelles. Subsequently, the short rod-like worm-like micelles gradually fuse into long linear worm-like micelles, and finally, the long linear worm-like micelles fuse into branched worm-like micelles.

Block copolymers with low arm numbers have shorter chain segments, which make them freer and the molecules tend to form more complex and less ordered aggregates. At this time, the morphology of linear worm-like micelles is often not fully stable, but more branched worms or more irregular

https://doi.org/10.1021/acsomega.5c00083
ACS Omega 2025, 10, 15419−15431

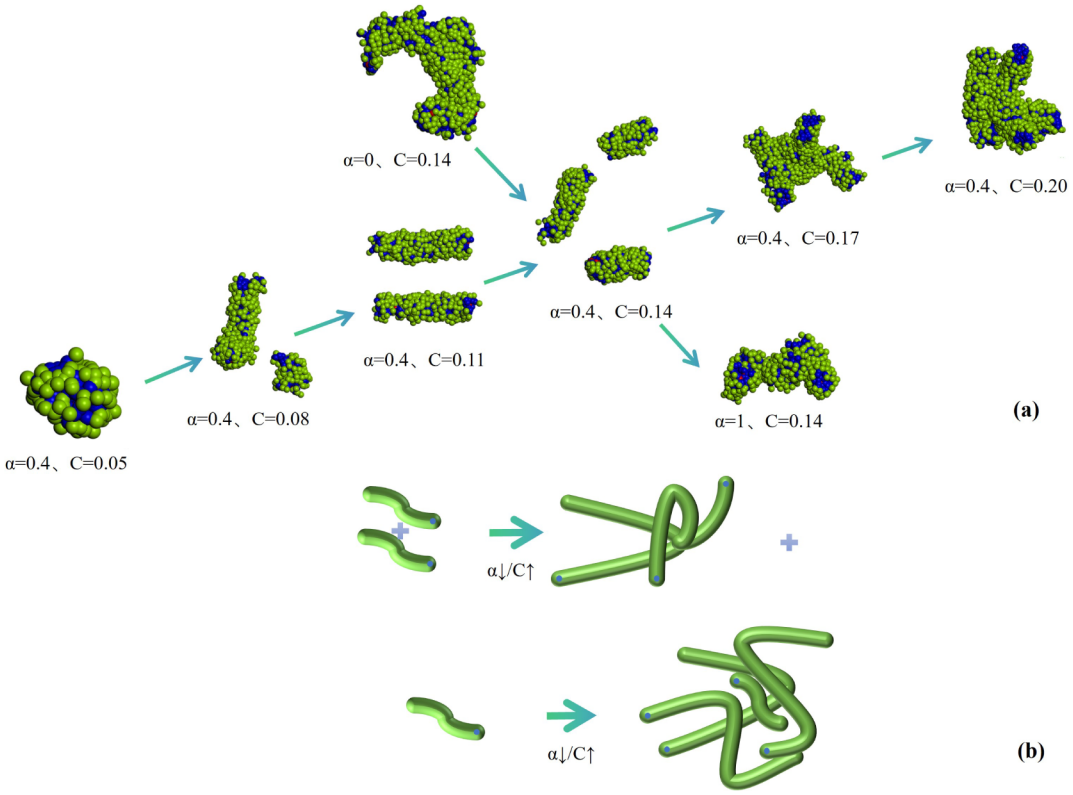

Figure 6. (a) Variation process of worm-like micelles at different concentrations of equal ionization degree and different ionization degrees of equal concentration; (b) schematic diagram of the formation process of branching worm-like micelles.

morphologies are formed; molecules with medium arm numbers have better geometric symmetry, and the length and rigidity of the molecular segments increase, which is conducive to the formation of linear worm-like structures. Within this range, molecules are more inclined to form stable worm-like structures through linear stacking in the long axis direction, thereby minimizing the free energy of the system; molecules with high arm numbers have higher degrees of freedom, more symmetrical geometry, longer and more rigid molecular segments, which prompt them to form more compact and symmetrical spherical micelles instead of linear worm-like structures. In addition, due to the lower surface energy of high-arm-number systems, spherical micelles can better minimize the free energy and thus dominate the self-assembly of the system.

In order to reveal the detailed paths of the above four self-assembly stages, representative intermediate states of all these stages are given in Figure 5. The first stage is the process of core−shell micelle formation. This process is similar to the self-assembly process of spherical PCL-CP molecules. The second stage is that the nearby small spherical micelles approach each other and then gradually fuse to form small short rod-type worm-like micelles. The third stage corresponds to the "head-to-head" fusion of short rod-type worm-like micelles and small spherical micelles, and then form long linear worm-like micelles. The fourth stage is that the long worm-like micelles fuse laterally to form branched worm-like micelles. In addition, in order to reveal the molecular stacking model inside the worm-like micelle, a cross-sectional view of a linear worm-like micelle is given. We can find that when the micelle is randomly cut into two parts, the micelle is completely separated into a core−shell structure. The hydrophobic PCL segment forms the micelle core, and the hydrophilic carboxyl arm covers the micelle surface to form the micelle shell. Furthermore, we can find that each PCL-CP molecule microphase separates into a cone, therefore, in order to form worm-like micelles, the PCL-CP molecules must transform from spheres to cones.

In addition, in order to study the effects of α and C on the shape of worm-like micelles, the change process of worm-like micelles at different concentrations of equal ionization and at different ionization degrees of equal concentration is shown in Figure 6a. When the ionization degree increases, α changes from 0 to 0.4 and then to 1, the micelles change from branched worms to short rod worms and then to spheres, which shows that the morphology of micelles is increasingly affected by electrostatic repulsion, thus forming individualized spheres; under the influence of the same ionization degree (α = 0.4), with the increase of concentration (C = 0.05−0.20), the van der Waals force between molecules becomes the dominant factor, resulting in the change of micelles from small spheres to worms and then to branched worms. Figure 6b provides a schematic diagram of the formation process of branched worm-like micelles.

Lamellar Micelles. Lamellar micelles mainly appear in systems with low arm numbers (S2, S3, S4), especially under conditions of lower ionization degree and medium concentration (α = 0−0.1 and C = 0.17−0.20 of S2 molecules, S3 molecules, S4 molecules (α = 0 −0.1 and C = 0.20) have low molecular flexibility and symmetry, which makes the molecules tend to be arranged along the plane to form a sheet-like structure. As the number of arms increases, the distribution range of lamellar micelles gradually decreases because the way the molecules are packed tends to form structures with higher

https://doi.org/10.1021/acsomega.5c00083
ACS Omega 2025, 10, 15419−15431

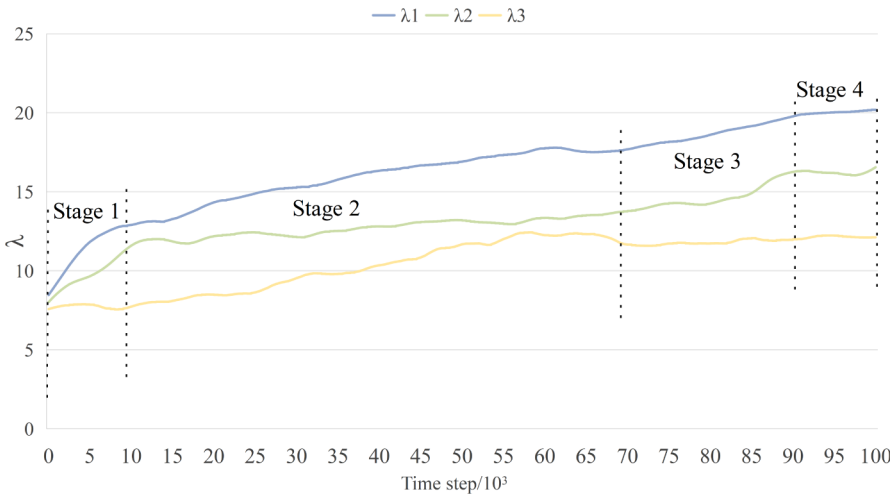

Figure 7. Real-time evolution of the three eigenvalues (λ_1, λ_2, λ_3) of the rotational radius squared tensor of the largest aggregates.

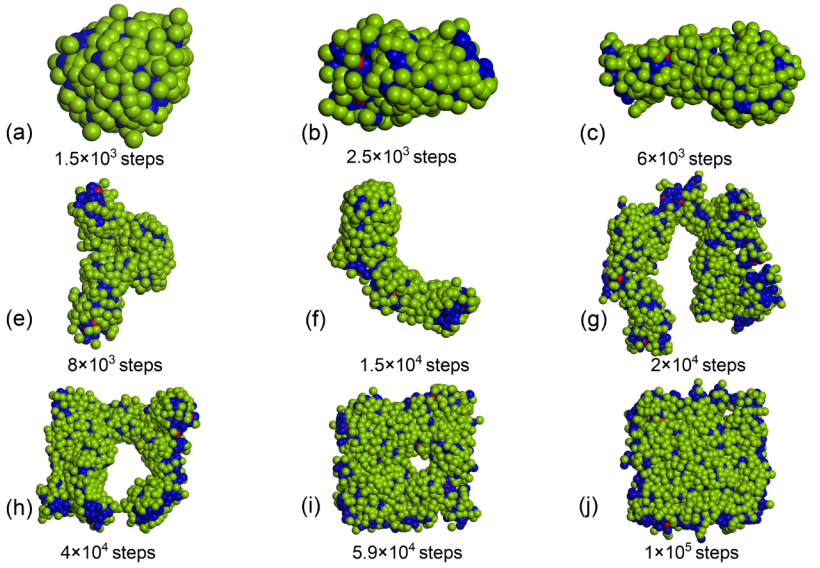

Figure 8. Corresponding morphology during the formation of layered micellar aggregates (a–j).

curvature, such as linear or spherical micelles. In systems with high arm numbers (S6, S8), the geometric symmetry and steric repulsion effects are significantly enhanced, and lamellar micelles are completely replaced by spherical and linear micelles, because the latter can more effectively minimize the free energy of the system and adapt to more complex structures. High symmetry molecular arrangement requirements. At the beginning, PCL-CP molecules were randomly distributed in the solution. They then aggregate into many small spherical micelles. Spherical micelles are sequentially aggregated into short worm-like micelles, long worm-like micelles and branched worm-like micelles. Subsequently, the worm-like micelles transform into complex branched ring micelles. Finally, the annular micelles close and fuse laterally to form a large lamellar micelle.

In order to reveal the formation process of sheet-like micelles, the rotation tensor radius (R_g) of S4-PCL-CP molecules is first constructed, as shown in eq 11, where n is the total number of beads in the aggregate, (x_i, y_i, z_i) is the position of the i-th bead, (x_{cm}, y_{cm}, z_{cm}) is the coordinates of the center of mass of the aggregate.

$$A = \begin{pmatrix} S_{xx} & S_{xy} & S_{xz} \\ S_{yx} & S_{yy} & S_{yz} \\ S_{zx} & S_{zy} & S_{zz} \end{pmatrix} \tag{14}$$

$$S_{xx} = \frac{1}{n}\sum_{i=1}^{n}(x_i - x_{cm})(x_i - x_{cm}) \tag{15}$$

$$S_{xy} = \frac{1}{n}\sum_{i=1}^{n}(x_i - x_{cm})(y_i - y_{cm}) \tag{16}$$

After diagonalizing the matrix, we can obtain the three eigenvalues λ_1, λ_2, and λ_3 of the square of the rotation tensor radius.

$$S = \begin{pmatrix} \lambda_1^2 & 0 & 0 \\ 0 & \lambda_2^2 & 0 \\ 0 & 0 & \lambda_3^2 \end{pmatrix} \tag{17}$$

https://doi.org/10.1021/acsomega.5c00083
ACS Omega 2025, 10, 15419−15431

Figure 7 gives the three eigenvalues of the square tensor of the radius of rotation of the largest aggregates in the S4 (α = 0.1 and C = 0.20) simulation box (λ_1, λ_2, λ_3) of the square tensor of the radius of rotation of the largest aggregate in the simulation box. Based on the trend of these eigenvalues, approximately four stages in the self-assembly process can be distinguished.

As shown in Figure 7, at the beginning, the values of λ_1, λ_2, and λ_3 are all relatively small values below $0-1.0 \times 10^4$ simulation steps. It is observed that λ_1 and λ_2 are rising synchronously, while λ_3 is steadily parallel. As shown in Figure 8, the first stage is explained by observing aggregates a and b to form small spherical micelles. Then in the simulation step of $1.0-6.8 \times 10^4$, it is observed that λ_1 and λ_3 are rising at an accelerated rate, while λ_2 is rising slowly. We found that irregular linear worm-like micelles are formed. Therefore, the second stage is characterized by multiple small spherical micelles gathering together to form linear worm-like micelles, which is found by observing the process from aggregate c to aggregate d and e. Then in the simulation step of $6.8-9.0 \times 10^4$, λ_1 and λ_2 both increase with the increase of simulation time, but λ_3 is slowly parallel. By directly observing the morphology of aggregates f and g, this stage corresponds to the complex interweaving of linear worm-like micelles to form branched worm-like micelles. In the fourth stage, λ_1, λ_2, and λ_3 rose steadily from the third stage to a constant value at present in the simulation step of $0.9-1.0 \times 10^5$. By observing the trajectory of this stage, we found that the branched worm-like micelles initially merged to form micelles with rings (from f to g and then to h), and finally closed to form lamellar micelles (aggregate i).

CONCLUSION

The self-assembly behavior of pH-responsive biobased polycaprolactone Star-Shaped block copolymers was thoroughly investigated by dissipative particle dynamics and molecular dynamics simulations. The results showed that the self-assembly morphology of the polymers was significantly regulated by terminal ionization degree, solution concentration and arm number. At low ionization degree, the aggregation effect of hydrophobic chain segments dominates, forming complex layered and branched worm-like micelles; with the increase of ionization degree and the enhancement of electrostatic repulsive force, the self-assembly gradually transitions to linear worm-like micelles and globular micelles with higher symmetry. Meanwhile, the increase in the number of arms enhances the intermolecular geometrical confinement and spatial repulsion effects, leading to the transition from complex to simple structures. This study systematically reveals the microphase separation mechanism of Star-Shaped block copolymers and their morphological evolution, providing a theoretical basis for regulating the self-assembly behavior of polymers. The low arm number system is suitable for the construction of complex two- or three-dimensional structures (e.g., membranes or reticular materials), while the high arm number system is suitable for the preparation of monodisperse particulate materials (e.g., drug carriers). These findings lay the foundation for further development of star block copolymers in the fields of drug delivery and smart materials.

ASSOCIATED CONTENT

Supporting Information

The Supporting Information is available free of charge at https://pubs.acs.org/doi/10.1021/acsomega.5c00083.

Dynamic self-assembly process video of S4-(α = 1.0, C = 0.20) PCL spherical micelles; spherical micelle self-assembly process (AVI)

AUTHOR INFORMATION

Corresponding Authors

Dengbang Jiang − *Green Preparation Technology of Biobased Materials National & Local joint Engineering Research Center, Yunnan Minzu University, Kunming 650500, China;* orcid.org/0000-0001-6035-3981; Email: 041814@ymu.edu.cn

Mingwei Yuan − *Green Preparation Technology of Biobased Materials National & Local joint Engineering Research Center, Yunnan Minzu University, Kunming 650500, China;* Email: 041808@ymu.edu.cn

Authors

Jiashu Pan − *Green Preparation Technology of Biobased Materials National & Local joint Engineering Research Center, Yunnan Minzu University, Kunming 650500, China;* orcid.org/0009-0009-1723-3226

Haiming Wang − *Affiliated School of Kunming NSAU Research Institute, Kunming 650500, China*

Zijun Liu − *Green Preparation Technology of Biobased Materials National & Local joint Engineering Research Center, Yunnan Minzu University, Kunming 650500, China*

Complete contact information is available at: https://pubs.acs.org/10.1021/acsomega.5c00083

Notes

The authors declare no competing financial interest.

ACKNOWLEDGMENTS

This study gratefully acknowledges the support of the State Local Joint Engineering Research Centre for Green Preparation Technology of Biobased Materials at Yunnan University for Nationalities, and the assistance of the State Ethnic Agricultural Committee and the Key Laboratory of Ethnic Medical Resource Chemistry of the Ministry of Education (Grant No. 2019MZY02).

REFERENCES

(1) Krishnan, M. R.; Lu, K.-Y.; Chiu, W.-Y.; Chen, I.-C.; Lin, J.-W.; Lo, T.-Y.; Georgopanos, P.; Avgeropoulos, A.; Lee, M.-C.; Ho, R.-M. Directed Self-Assembly of Star-Block Copolymers by Topographic Nanopatterns through Nucleation and Growth Mechanism. *Small* **2018**, *14* (16), 1704005.

(2) Sternhagen, G. L.; Gupta, S.; Zhang, Y.; John, V.; Schneider, G. J.; Zhang, D. Solution Self-Assemblies of Sequence-Defined Ionic Peptoid Block Copolymers. *J. Am. Chem. Soc.* **2018**, *140* (11), 4100−4109.

(3) Li, L.; Li, W. Effect of branching architecture on the self-assembly of symmetric ABC-type block terpolymers. *Giant* **2021**, *7*, 100065.

(4) Wang, R.; Zhu, W.; Zhang, L.; Sheng, X.; Tan, J. Synthesis of Self-assembled Star/Linear Block Copolymer Blends via Aqueous RAFT Dispersion Polymerization. *Chin. J. Chem.* **2024**, *42* (14), 1606−1614.

(5) Buwalda, S.; Al Samad, A.; El Jundi, A.; Bethry, A.; Bakkour, Y.; Coudane, J.; Nottelet, B. Stabilization of poly(ethylene glycol)-poly(ε-caprolactone) star block copolymer micelles via aromatic groups for improved drug delivery properties. *J. Colloid Interface Sci.* **2018**, *514*, 468−478.
(6) Yao, X.; Cao, X.; He, J.; Hao, L.; Chen, H.; Li, X.; Huang, W. Controlled Fabrication of Unimolecular Micelles as Versatile Nanoplatform for Multifunctional Applications. *Small* **2024**, *20* (48), 2405816.
(7) Ghezzi, M.; Pescina, S.; Padula, C.; Santi, P.; Del Favero, E.; Cantù, L.; Nicoli, S. Polymeric micelles in drug delivery: An insight of the techniques for their characterization and assessment in biorelevant conditions. *J. Controlled Release* **2021**, *332*, 312−336.
(8) Lim, C.; Ramsey, J. D.; Hwang, D.; Teixeira, S. C. M.; Poon, C.-D.; Strauss, J. D.; Rosen, E. P.; Sokolsky-Papkov, M.; Kabanov, A. V. Drug-Dependent Morphological Transitions in Spherical and Worm-Like Polymeric Micelles Define Stability and Pharmacological Performance of Micellar Drugs. *Small* **2021**, *18* (4), 2103552.
(9) Qiu, M.; Ouyang, J.; Sun, H.; Meng, F.; Cheng, R.; Zhang, J.; Cheng, L.; Lan, Q.; Deng, C.; Zhong, Z. Correction to "Biodegradable Micelles Based on Poly(ethylene glycol)-b-polylipopeptide Copolymer: A Robust and Versatile Nanoplatform for Anticancer Drug Delivery". *ACS Appl. Mater. Interfaces* **2021**, *13* (6), 7822.
(10) Augustine, D.; Hadjichristidis, N.; Gnanou, Y.; Feng, X. Hydrophilic Stars, Amphiphilic Star Block Copolymers, and Miktoarm Stars with Degradable Polycarbonate Cores. *Macromolecules* **2020**, *53* (3), 895−904.
(11) Grosjean, M.; Gangolphe, L.; Déjean, S.; Hunger, S.; Bethry, A.; Bossard, F.; Garric, X.; Nottelet, B. Dual-Crosslinked Degradable Elastomeric Networks With Self-Healing Properties: Bringing Multi-(catechol) Star-Block Copolymers into Play. *ACS Appl. Mater. Interfaces* **2023**, *15* (1), 2077−2091.
(12) Chen, Y. C.; Chang, C. J.; Hsiue, G. H.; Chiang, Y. T. Doxorubicin-Loaded Mixed Micelles Using Degradable Graft and Diblock Copolymers to Enhance Anticancer Sensitivity. *Cancers* **2021**, *13*, 3816.
(13) Zhang, Y.; Guan, T.; Han, G.; Guo, T.; Zhang, W. Star Block Copolymer Nanoassemblies: Block Sequence is All-Important. *Macromolecules* **2019**, *52* (2), 718−728.
(14) Szymusiak, M.; Kalkowski, J.; Luo, H.; Donovan, A. J.; Zhang, P.; Liu, C.; Shang, W.; Irving, T.; Herrera-Alonso, M.; Liu, Y. Core−Shell Structure and Aggregation Number of Micelles Composed of Amphiphilic Block Copolymers and Amphiphilic Heterografted Polymer Brushes Determined by Small-Angle X-ray Scattering. *ACS Macro Lett.* **2017**, *6* (9), 1005−1012.
(15) Kozawa, S. K.; Matsumoto, K.; Suzuki, A.; Sawamoto, M.; Terashima, T. Self-assembly of amphiphilic ABA random triblock copolymers in water. *J. Polym. Sci., Part A: Polym. Chem.* **2019**, *57* (3), 313−321.
(16) Bahadori, F.; Dag, A.; Durmaz, H.; Cakir, N.; Onyuksel, H.; Tunca, U.; Topcu, G.; Hizal, G. Synthesis and Characterization of Biodegradable Amphiphilic Star and Y-Shaped Block Copolymers as Potential Carriers for Vinorelbine. *Polymers* **2014**, *6*, 214−242.
(17) Leong, J.; Tay, J.; Yang, S.; Yang, C.; Tan, E. W. P.; Wang, Y.; Tan, B. Q.; Hor, S.; Chua, Y. H.; Tan, J. P. K.; et al. Nanocomplexes of Biodegradable Anticancer Macromolecules: Prolonged Plasma Half-Life, Reduced Toxicity, and Increased Tumor Targeting. *Adv. Healthcare Mater.* **2023**, *12* (19), 2201560.
(18) Wang, H.; Xu, L.; Chen, X. Z.; Ullah, A. Tunable self-assembly of lipid-based block polymeric micelles with temperature-sensitive poly(vinylcaprolactam) shell for effective anticancer drug delivery. *Eur. Polym. J.* **2024**, *206*, 112795.
(19) Akimoto, J.; Nakayama, M.; Okano, T. Temperature-responsive polymeric micelles for optimizing drug targeting to solid tumors. *J. Controlled Release* **2014**, *193*, 2−8.
(20) Lin, W.; Yao, N.; Qian, L.; Zhang, X.; Chen, Q.; Wang, J.; Zhang, L. pH-responsive unimolecular micelle-gold nanoparticles-drug nanohybrid system for cancer theranostics. *Acta Biomater.* **2017**, *58*, 455−465.
(21) Tan, L.; Fan, J.; Zhou, Y.; Xiong, D.; Duan, M.; Hu, D.; Wu, Z. Preparation of reversible cross-linked amphiphilic polymeric micelles with pH-responsive behavior for smart drug delivery. *RSC Adv.* **2023**, *13* (40), 28165−28178.
(22) Cao, H.; Yi, M.; Wei, H.; Zhang, S. Construction of Folate-Conjugated and pH-Responsive Cell Membrane Mimetic Mixed Micelles for Desirable DOX Release and Enhanced Tumor-Cellular Target. *Langmuir* **2022**, *38* (31), 9546−9555.
(23) Shen, Y.; Guo, Q.; Zhang, T.; Wang, L.; Chen, S.; Lan, X.; Li, Q.; Xiao, H. Zwitterionic dendrimer self-assembled nanodrugs with high drug loading for enhanced anti-tumor ability. *Colloids Surf., B* **2023**, *231*, 113574.
(24) Callari, M.; Wong, S.; Lu, H.; Aldrich-Wright, J.; de Souza, P.; Stenzel, M. H. Drug induced self-assembly of triblock copolymers into polymersomes for the synergistic dual-drug delivery of platinum drugs and paclitaxel. *Polym. Chem.* **2017**, *8* (40), 6289−6299.
(25) Shen, C.; Li, J.; Li, C.; Wang, L.; Wang, Z.; Zhang, K.; Li, Z.; Cao, L.; Chen, L. Construction and antitumor evaluation of stimulus-responsive dual-drug micelles based on computer simulation. *J. Drug Delivery Sci. Technol.* **2024**, *93*, 105366.
(26) Li, S.; Yu, C.; Zhou, Y. Phase diagrams, mechanisms and unique characteristics of alternating-structured polymer self-assembly via simulations. *Sci. China: Chem.* **2019**, *62* (2), 226−237.
(27) Yang, Y.; Qiu, F.; Tang, P.; Zhang, H. Applications of self-consistent field theory in polymer systems. *Sci. China, Ser. B* **2006**, *49* (1), 21−43.
(28) Dalsin, S. J.; Rions-Maehren, T. G.; Beam, M. D.; Bates, F. S.; Hillmyer, M. A.; Matsen, M. W. Bottlebrush Block Polymers: Quantitative Theory and Experiments. *ACS Nano* **2015**, *9* (12), 12233−12245.
(29) Hao, L.; Lin, L.; Zhou, J. pH-Responsive Zwitterionic Copolymer DHA−PBLG−PCB for Targeted Drug Delivery: A Computer Simulation Study. *Langmuir* **2019**, *35* (5), 1944−1953.
(30) Xu, J.; Wen, L.; Zhang, F.; Lin, W.; Zhang, L. Self-assembly of cyclic grafted copolymers with rigid rings and their potential as drug nanocarriers. *J. Colloid Interface Sci.* **2021**, *597*, 114−125.
(31) Yang, C.; Yin, L.; Yuan, C.; Liu, W.; Guo, J.; Shuttleworth, P. S.; Yue, H.; Lin, W. DPD simulations and experimental study on reduction-sensitive polymeric micelles self-assembled from PCL-SS-PPEGMA for doxorubicin controlled release. *Colloids Surf., B* **2021**, *204*, 111797.
(32) Xu, J.; Wang, Z.; Gao, J.; Li, C.; Sun, S.; Hu, S. Dissipative particle dynamics simulations reveal the pH-driven micellar transition pathway of monorhamnolipids. *J. Colloid Interface Sci.* **2017**, *506*, 493−503.
(33) Zheng, L. S.; Yang, Y. Q.; Guo, X. D.; Sun, Y.; Qian, Y.; Zhang, L. J. Mesoscopic simulations on the aggregation behavior of pH-responsive polymeric micelles for drug delivery. *J. Colloid Interface Sci.* **2011**, *363* (1), 114−121.
(34) Pranav, U.; Malhotra, M.; Pathan, S.; Jayakannan, M. Structural Engineering of Star Block Biodegradable Polymer Unimolecular Micelles for Drug Delivery in Cancer Cells. *ACS Biomater. Sci. Eng.* **2023**, *9* (2), 743−759.
(35) Hoogerbrugge, P. J.; Koelman, J. Simulating microscopic hydrodynamic phenomena with dissipative particle dynamics. *Europhys. Lett.* **1992**, *19* (3), 155−160.
(36) Khadilkar, M. R.; Escobedo, F. A. Self-assembly of binary space-tessellating compounds. *J. Chem. Phys.* **2012**, *137* (19), 194907.
(37) Padmanabhan, P.; Martinez-Veracoechea, F. J.; Araque, J. C.; Escobedo, F. A. A theoretical and simulation study of the self-assembly of a binary blend of diblock copolymers. *J. Chem. Phys.* **2012**, *136* (23), 234905.
(38) Xiao, M.; Xia, G.; Wang, R.; Xie, D. Controlling the self-assembly pathways of amphiphilic block copolymers into vesicles. *Soft Matter* **2012**, *8* (30), 7865−7874.
(39) Huang, J.; Wang, Y.; Laradji, M. Flow Control by Smart Nanofluidic Channels: A Dissipative Particle Dynamics Simulation. *Macromolecules* **2006**, *39* (16), 5546−5554.

https://doi.org/10.1021/acsomega.5c00083
ACS Omega 2025, 10, 15419−15431

(40) Groot, R. D.; Warren, P. B. Dissipative Particle Dynamics: Bridging the Gap between Atomistic and Mesoscopic Simulation. *J. Chem. Phys.* **1997**, *107*, 4423−4435.
(41) Posel, Z.; Limpouchová, Z.; Šindelka, K.; Lísal, M.; Procházka, K. Dissipative Particle Dynamics Study of the pH-Dependent Behavior of Poly(2-vinylpyridine)-block-poly(ethylene oxide) Diblock Copolymer in Aqueous Buffers. *Macromolecules* **2014**, *47* (7), 2503−2514.
(42) Lísal, M.; Limpouchová, Z.; Procházka, K. The Self-Assembly of Copolymers with One Hydrophobic and One Polyelectrolyte Block in Aqueous Media: A Dissipative Particle Dynamics Study. *Phys. Chem. Chem. Phys.* **2016**, *1*, 16127−16136.

https://doi.org/10.1021/acsomega.5c00083
ACS Omega 2025, 10, 15419−15431